




Long Wavelength InAs/InAsSb Infrared Superlattice Challenges: A Theoretical Investigation

DAVID Z. TING ^{1,2}, AREZOU KHOSHAKHLAGH,¹
ALEXANDER SOIBEL,¹ and SARATH D. GUNAPALA¹

1.—Jet Propulsion Laboratory, California Institute of Technology, M/S 302-231, 4800 Oak Grove Drive, Pasadena, CA 91109-8099, USA. 2.—e-mail: David.Z.Ting@jpl.nasa.gov

InAs/InAsSb type-II superlattice focal plane arrays that demonstrate high operability and uniformity with cutoffs ranging from 5 μm to 13 μm have already been demonstrated. Compared to InAs/GaSb, the InAs/InAsSb superlattice is easier to grow and has longer minority carrier lifetimes, but requires a longer superlattice period to achieve long or very long wavelength cutoffs. A longer type-II superlattice period leads to smaller absorption coefficients and larger growth-direction hole conductivity effective masses. We explore by theoretical modeling some of the ideas aimed at addressing these challenges for the long and very long wavelength InAs/InAsSb superlattice. Increasing the Sb fraction in the InAsSb alloy can reduce the InAs/InAsSb superlattice period significantly, but this benefit can be negated by Sb segregation. Thin AlAsSb barrier layers can be inserted in InAs/InAsSb to form polytype W, M, and N superlattices in order to increase electron–hole wavefunction overlap for stronger optical absorption. However, this strategy can be unfavorable since the AlAsSb barriers increase the band gap, and thereby increase the superlattice period required to reach a given cutoff wavelength. Metamorphic growth on virtual substrates with larger lattice constants than GaSb can decrease the superlattice period needed to reach a specified cutoff wavelength, but this benefit should be weighed against the need for metamorphic buffer growth and the resulting higher defect density.

Key words: Infrared detector, unipolar barrier, type-II superlattice, InAs/InAsSb superlattice

INTRODUCTION

The InAs/InAsSb (gallium-free) type-II strained-layer superlattice (T2SLS) has emerged as an alternative to the more established InAs/GaSb type-II superlattice (T2SL) for infrared detector applications. We have previously documented the

history of the InAs/InAsSb T2SLS,¹ as well as the development of InAs/InAsSb T2SLS infrared detectors at the NASA Jet Propulsion Laboratory (JPL).² InAs/InAsSb T2SLS focal plane arrays (FPAs) with high operability and uniformity have been demonstrated in mid-wavelength infrared (MWIR), long wavelength infrared (LWIR), and very long wavelength infrared (VLWIR)¹; focal plane arrays with cutoffs ranging from 5 μm to 13 μm were briefly discussed in Ref. 1. In particular, FPAs based on the mid-wavelength (MW) InAs/InAsSb T2SLS unipolar barrier infrared detector^{3,4} have demonstrated significantly higher operating temperature than their InSb counterparts while retaining the same III–V semiconductor manufacturability benefits, thus

(Received January 29, 2020; accepted July 21, 2020; published online August 9, 2020)

establishing the InAs/InAsSb T2SLS as an important infrared detector material. Specifically, while ion-implanted planar InSb FPAs and molecular beam epitaxy (MBE) grown epi-InSb FPAs typically operate at 80 K and 95–100 K,^{5,6} respectively, InAs/InAsSb T2SLS FPAs with comparable cutoff wavelength operate well at 160 K.^{3,4} Compared to the InAs/GaSb T2SL, InAs/InAsSb T2SLS is easier to grow,⁷ and has demonstrated longer minority carrier lifetimes.^{8–10} For instance, the MW InAs/GaSb T2SL minority carrier lifetime has been reported at ~ 80 ns,¹¹ while non-intentionally doped MW InAs/InAsSb T2SLS has exhibited minority carrier lifetime values from $1.8 \mu\text{s}$ ¹⁰ to $9 \mu\text{s}$,⁹ with a Shockley–Read–Hall (SRH) lifetime of $\sim 10 \mu\text{s}$.¹⁰ However, (V)LWIR InAs/InAsSb T2SLS have smaller absorption coefficients and lower quantum efficiency than InAs/GaSb T2SL.^{12,13} Vurgaftman et al. calculated the absorption coefficients for LWIR superlattices with band gaps of ~ 0.1 eV (corresponding to cutoff wavelengths of $\lambda_{\text{cutoff}} = 10\text{--}12 \mu\text{m}$) and showed that the InAs/InAsSb T2SLS absorption coefficient is approximately half as large as that for the InAs/GaSb T2SL¹³; at $\lambda = 8 \mu\text{m}$, the absorption coefficients are $\sim 1250 \text{ cm}^{-1}$ and $\sim 700 \text{ cm}^{-1}$ for the InAs/GaSb (70 \AA period) and the InAs/InAsSb (125 \AA period) superlattices, respectively. Klipstein et al. modeled the dependence of LWIR superlattice detector spectral quantum efficiency (QE) on diffusion length, and concluded that even for a very large diffusion length, the InAs/InAsSb T2SLS has a significantly lower QE than the InAs/GaSb T2SL because of its weaker absorption coefficient.¹² The work also showed an example of the strong QE dependence on the diffusion length in the LWIR InAs/InAsSb T2SLS XbN detector; for a $9.7\text{-}\mu\text{m}$ cutoff detector with a $5 \mu\text{m}$ thick n -type absorber, the QE at $8.5 \mu\text{m}$ is 40% for a $5\text{-}\mu\text{m}$ hole diffusion length, but drops to 10% for a $1\text{-}\mu\text{m}$ hole diffusion length.¹² Meanwhile, theoretical results have also shown that in the long wavelength regime the InAs/InAsSb T2SLS has larger growth-direction hole conductivity effective mass ($m_{p,z}^{**}$) compared to the InAs/GaSb T2SL, and that $m_{p,z}^{**}$ can increase rapidly with the cutoff wavelength^{14,15}; this also is unfavorable for attaining high QE since the diffusion length is inversely proportional to the square root of the conductivity effective mass.¹⁴ Therefore, achieving high QE in (V)LWIR InAs/InAsSb T2SLS FPAs has been more challenging. In this paper we explore theoretically some ideas for addressing these challenges. We use an enhanced effective bond orbital model (EBOM)^{16,17} in our calculations, with material parameters taken from the Vurgaftman et al.¹⁸ In the sections that follow, we examine the role of InAsSb alloy fraction, the effect of antimony segregation, wave function engineering in W, M, and N polytype superlattices, and metamorphic growth.

PERIODICITY OF INAS/INASSB AND INAS/GASB SUPERLATTICES

The smaller absorption coefficients and the larger hole effective masses of (V)LWIR InAs/InAsSb T2SLS can be traced to the fact that a longer superlattice period is required to achieve the same band gap (or the corresponding detector cutoff wavelength) than the InAs/GaSb T2SL. Figure 1 shows the energy band diagrams for an InAs/InAsSb T2SLS and an InAs/GaSb T2SL, with calculated band gaps of 116 meV and 113 meV, respectively. The energy levels of the lowest conduction band (c1), highest heavy hole (hh1), and highest light hole (lh1), and c1 and hh1 probability densities are also shown. Although the two superlattices have approximately the same band gap, the InAs/InAsSb T2SLS has a much longer period (35 versus 22 monolayers, or MLs). There are two reasons. First, while both superlattices use InAs electron quantum wells, they differ in hole quantum wells. The GaSb valence band edge is noticeably higher than the InAsSb valence band edge; this pulls the superlattice valence subband edge (hh1) higher, and makes it easier to achieve smaller superlattice band gap. Second, for InAs/InAsSb T2SLS grown on a GaSb substrate, typically the InAs layer is under slight tensile strain while InAsSb is under relatively high compressive strain. Therefore, a comparatively thick InAs layer is required to strain balance against the InAsSb layer in the InAs/InAsSb T2SLS, even though increasing the InAs layer thickness contributes only marginally to reducing the (V)LWIR superlattice band gap. Thicker InAs layers lead to stronger isolation of the InAsSb valence band quantum wells, resulting in larger growth-direction hole effective masses. Large growth-direction hole effective masses limit the hole diffusion length and quantum efficiency in detectors with n -type absorber. Having thicker InAs layers in InAs/InAsSb superlattice also decreases the fraction of c1 probability density tailing into the InAsSb layers where the hh1 wave function is localized (see Fig. 1), thereby reducing the electron–hole wave function overlap, and thus leading to weaker oscillator strength and smaller absorption coefficient.

As discussed above, the period required to reach a given band gap (E_g), or the corresponding cutoff wavelength ($\lambda_{\text{cutoff}} = hc/E_g$), is a simple but often informative quantity for a type-II superlattice. We will make use of this frequently in this paper when we compare different types of superlattices. Figure 2 shows the calculated cutoff wavelength as a function of superlattice period for a set of (m,n)-InAs/InAsSb T2SLS (m and n , respectively, are the number of monolayers of InAs and InAsSb in each superlattice period) with $m/n = 4$, and a set of (m,n)-InAs/GaSb T2SL with $n = 7$. The cutoff wavelength is derived from the calculated superlattice band gap using the relationship $\lambda_{\text{cutoff}} (\mu\text{m}) = 1.24/E_g$ (eV). In the mid-wavelength infrared (MWIR) range, the two

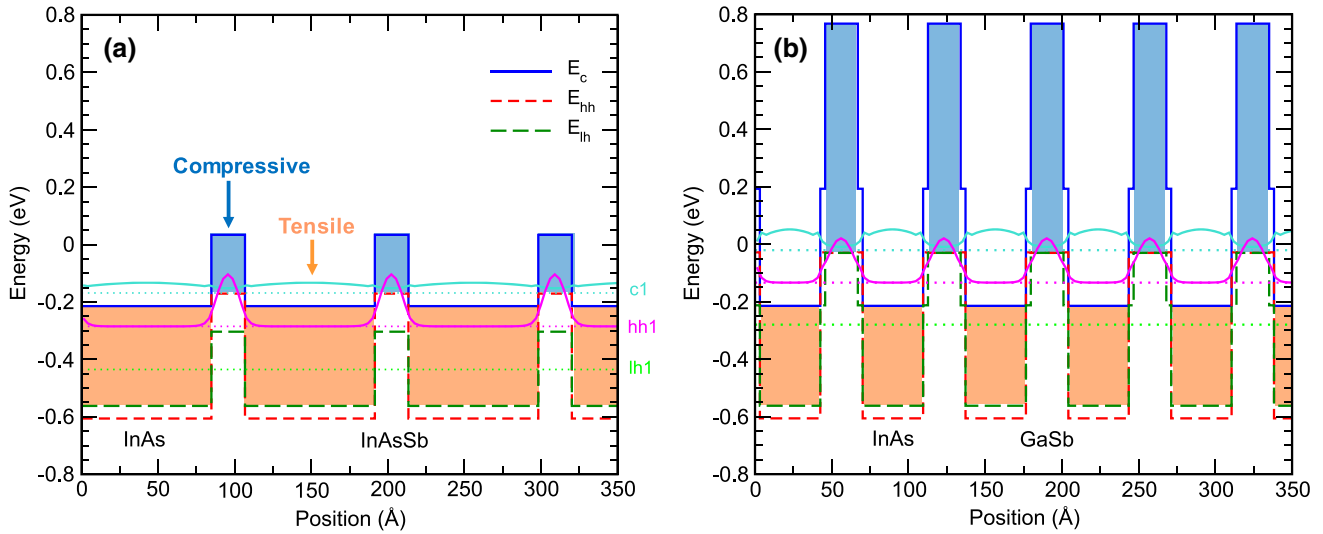


Fig. 1. Energy band diagrams, the superlattice zone-center $c1$, $hh1$, and $lh1$ energy levels (dotted lines), and $c1$ and $hh1$ state probability densities (solid lines) for: (a) the (28,7)-InAs/InAs_{0.5}Sb_{0.5} superlattice, and (b) the (15,7)-InAs/GaSb superlattice on GaSb substrate at 100 K.

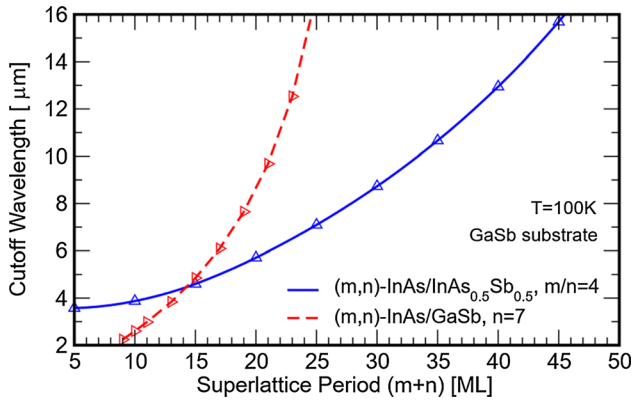


Fig. 2. Calculated cutoff wavelength for the (m,n) -InAs/InAs_{0.5}Sb_{0.5} superlattices with $m/n = 4$, and for the (m,n) -InAs/GaSb superlattice with $n = 7$, as functions of superlattice period in monolayers (MLs).

sets of superlattices have comparable periods. As the cutoff wavelength increases, the periodicity disadvantage of the InAs/InAsSb T2SLS becomes more pronounced. This is one of the main challenges for the long-wavelength InAs/InAsSb T2SLS.

THE ROLE OF INASSB ALLOY FRACTION

We mentioned in the last section that one reason we can reach the same (V)LWIR band gap with a shorter period in the InAs/GaSb T2SL than in the (typical) InAs/InAsSb T2SLS is because the GaSb valence band edge is higher than that of the InAsSb (at typical alloy fraction); a higher valence band edge for the hole quantum well pulls the $hh1$ state closer to the $c1$ state in the InAs quantum well. In fact, we can consider the difference between the hole quantum well valence band edge and the electron quantum well conduction band edge a measure of the strength of “type-II-ness”; a larger difference makes it easier to achieve a smaller type-II

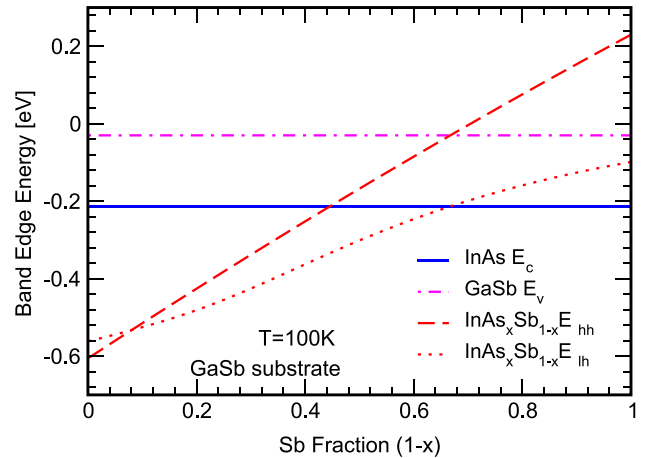


Fig. 3. Heavy-hole and light-hole band edges of InAsSb as functions of alloy composition, the conduction band edge of InAs, and the valence band edge of GaSb, where InAs, InAsSb are strained to the GaSb substrate lattice constant.

superlattice band gap. Figure 3 shows that the heavy-hole (hh) and light-hole (lh) positions as functions of alloy composition for InAsSb strained to the GaSb substrate. As we are working with compressively strained InAs _{x} Sb _{$1-x$} ($x < 0.92$), the hh position is the relevant valence edge. Figure 3 show the InAsSb hh band edge (E_{hh}^{InAsSb}) rises as the Sb fraction increases; for Sb fraction larger than 67%, E_{hh}^{InAsSb} is actually higher than the GaSb valence band edge (E_v^{GaSb}). This suggests that we should examine InAs/InAsSb T2SLS made from InAsSb alloy with high Sb fraction. Figure 4 shows the calculated cutoff wavelength as function of superlattice period for families of (m,n) -InAs/InAsSb superlattices with different m/n ratios. Note that superlattices with larger m/n ratios use InAsSb with higher Sb fraction (more compressively strained) for strain balancing. Figure 4 shows that

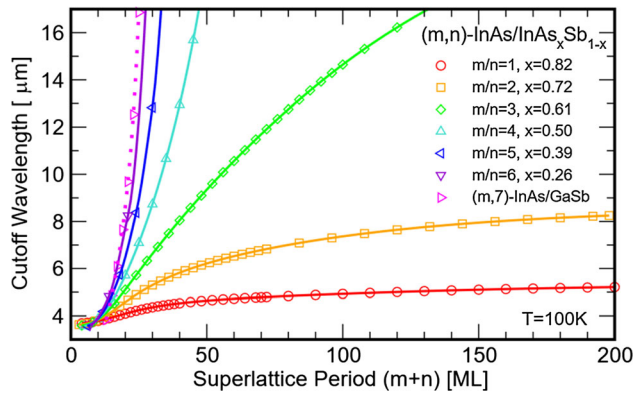


Fig. 4. Calculated cutoff wavelength for several families of InAs/InAsSb superlattices (solid lines) as functions of superlattice period in monolayers. The results for a set of InAs/GaSb superlattice (dotted line) is also included for comparison.

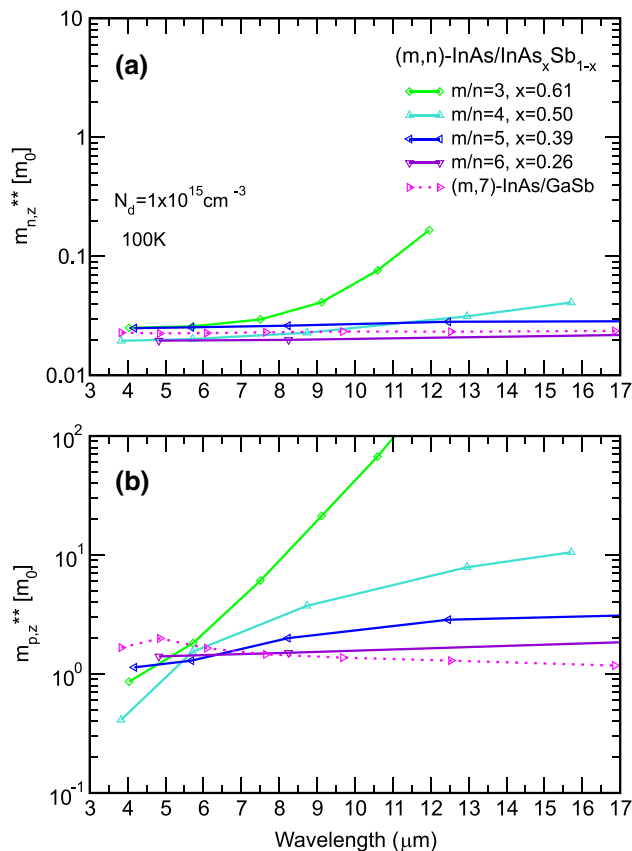


Fig. 5. Growth-direction (a) electron and (b) hole conductivity effective masses for several families of InAs/InAsSb superlattices (solid lines), and a set of InAs/GaSb superlattices (dotted lines).

indeed InAs/InAsSb T2SLS with higher Sb fraction can reach a specified cutoff wavelength with shorter superlattice period. At an Sb fraction of 74%, the InAs/InAsSb T2SLS nearly matches the InAs/GaSb T2SL in the cutoff wavelength versus superlattice period characteristics.

Figure 5 shows the calculated electron and hole conductivity effective masses along the growth

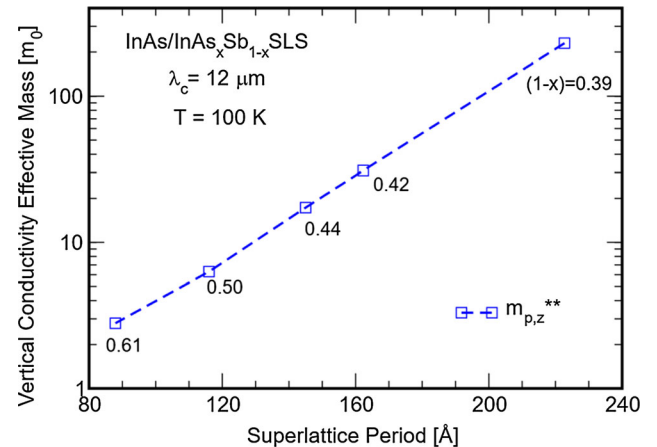


Fig. 6. Growth-direction hole conductivity effective mass $m_{p,z}^{**}$ as a function of superlattice period for several 12- μm cutoff InAs/InAsSb superlattices of different designs.

direction ($m_{n,z}^{**}$ and $m_{p,z}^{**}$, respectively) as functions of cutoff wavelengths. The conductivity effective masses are thermally averaged quantities which take into account the anisotropy and non-parabolicity in the superlattice band structure; detailed discussions are found in Refs. 14 and 15. In general, the electron effective mass $m_{n,z}^{**}$ is quite small in InAs/InAsSb T2SLS since the c1 wavefunctions are only weakly confined in the relative shallow conduction band quantum wells. On the other hand, $m_{p,z}^{**}$ can be very large when the InAsSb hole quantum wells are separated by wider InAs layer. Here higher Sb fraction decreases the InAs/InAsSb T2SLS period and is, therefore, especially helpful in reducing the growth-direction hole conductivity effective masses. Figure 6 summarizes the key results of this section by comparing a set of InAs/InAsSb superlattices, all with 12- μm cutoff wavelength, but with different Sb fractions. With increasing Sb fraction the superlattice period decreases, which in turn leads to an exponential decrease in the growth-direction hole conductivity effective mass.

Although using InAsSb alloy with high Sb fraction appears to be an appealing approach for addressing the issues of low absorption coefficient and large growth direction conductivity effective masses in (V)LWIR InAs/InAsSb T2SLS, there are practical concerns. One reason the Sb fraction cannot be very high is that the high Sb-fraction InAsSb layer would be under very high compressive strain, which could lead to (partial) relaxation. Another reason is antimony segregation, which we discuss next.

ANTIMONY SEGREGATION

For MBE growth, growing InAsSb with higher Sb fraction requires higher Sb flux, which leaves higher residual amount of Sb in the growth chamber after the Sb shutter is closed for InAs growth. This in turn could lead to an increase in un-intended Sb

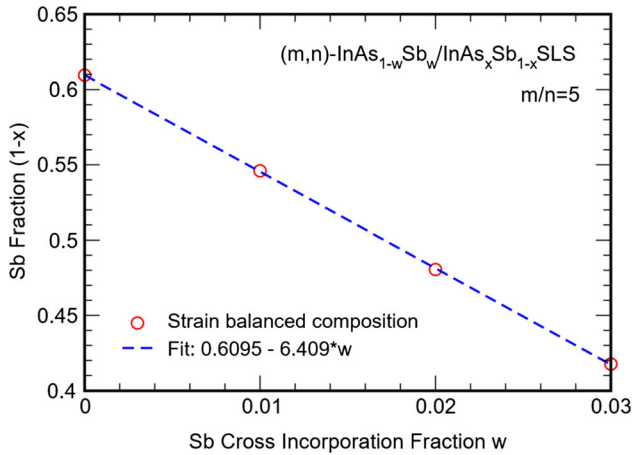


Fig. 7. For the (m,n) - $\text{InAs}_{1-w}\text{Sb}_w/\text{InAs}_x\text{Sb}_{1-x}$ superlattice with $m/n = 5$, the InAsSb alloy fraction x required for strain balancing is plotted as a function of w .

cross-incorporation into the binary InAs layer. Antimony segregation in $\text{InAs}/\text{InAsSb}$ T2SLS, where Sb atoms from InAsSb layers are incorporated into the nominally binary InAs layers, has been investigated by molecular dynamics growth modeling,¹⁹ and has also been observed experimentally.^{20–22} Modeling results show that Sb appears to have a Gaussian distribution centered about the middle of the InAsSb layer.¹⁹ Here we model the effect of Sb segregation using a simplified structure where each of the two layers in the superlattice period consists of InAsSb of fixed composition. Specifically, we consider the $\text{InAs}_{1-w}\text{Sb}_w/\text{InAs}_x\text{Sb}_{1-x}$ superlattice where a small fraction (“ w ”) of Sb is now incorporated into the nominally binary InAs layer in the ideal $\text{InAs}/\text{InAsSb}$ superlattice. In superlattice growth, we would typically specify the thickness ratio of the two constituent layers in the superlattice period, and at the same time require strain balancing. In our model, for a fixed layer width ratio, we selected a cross-incorporation fraction w , and adjust the Sb fraction $(1-x)$ in $\text{InAs}_x\text{Sb}_{1-x}$ to maintain strain balancing with respect to the GaSb substrate. Figure 7 shows that as we increase w , we must lower the Sb fraction $(1-x)$ to maintain strain balancing. This, in turn, increases the superlattice period needed to achieve a targeted cutoff wavelength, and also dramatically increases the growth-direction hole conductivity effective mass, as shown in Fig. 8. Therefore, while in theory $\text{InAs}/\text{InAsSb}$ T2SLS with high Sb fraction has more favorable properties, unintended Sb segregation can greatly diminish the effectiveness.

WAVEFUNCTION ENGINEERING IN POLYTYPE SUPERLATTICES

Polytype superlattices²³ such as the “W”,²⁴ “M”,²⁵ and “N”²⁶ structures have been used for improving oscillator strength over the basic InAs/GaSb T2SL. Here we investigate the analogous Ga -free

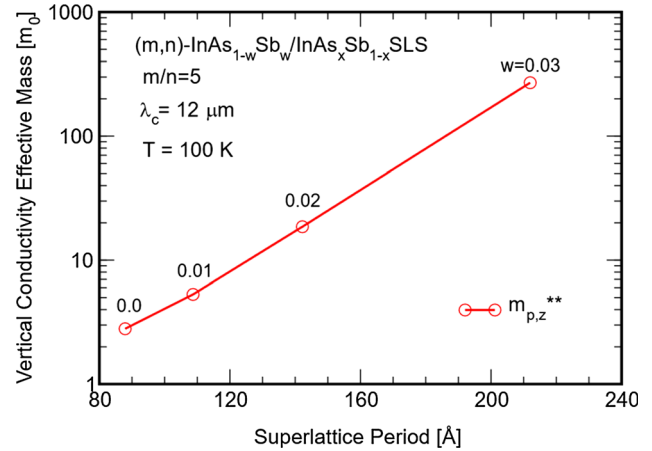


Fig. 8. Growth-direction hole conductivity effective mass $m_{p,z}^{**}$ versus superlattice period for a set of $12\text{-}\mu\text{m}$ cutoff (m,n) - $\text{InAs}_{1-w}\text{Sb}_w/\text{InAs}_x\text{Sb}_{1-x}$ superlattices, with $m/n = 5$ and at various values of composition w , strain-balanced with respect to the GaSb substrate.

structures by inserting thin layers of $\text{Al}_{0.08}\text{As}_{0.92}\text{Sb}$ (lattice-matched to GaSb substrate) into the $\text{InAs}/\text{InAsSb}$ T2SLS. Figures 9 and 10 show the energy band diagrams, the lowest conduction subband (c1) and the highest valence subband (hh1) state energy levels and the associated probability densities for an $\text{InAs}/\text{InAsSb}$ T2SLS and the corresponding W, M, and N superlattices. For the W superlattice (W-SL), the insertion of a thin AlAsSb layer in the middle of each InAs electron quantum well pushes the c1 wavefunction towards the InAsSb hole quantum wells for stronger overlap with the hh1 wavefunction. For the M-SL, insertion of a thin AlAsSb layer in the middle of each InAsSb hole quantum well pushes the hh1 wavefunction out for stronger overlap with the c1 wavefunction. For the N-SL, the AlAsSb barrier inserted at the InAs - InAsSb interfaces pushes the c1 electron wavefunction toward the unmodified InAsSb - InAs interfaces for slightly improved c1-hh1 wavefunction overlap.

Figure 11 shows the c1 and hh1 energy levels as functions of superlattice period for a family of (m,n) - $\text{InAs}/\text{InAs}_{0.5}\text{Sb}_{0.5}$ superlattices, with $m/n = 4$, and the corresponding W-SL, M-SL, and N-SL families. For the W-SL, the AlAsSb electron barrier centered in the InAs electron quantum well raises the c1 level but has little effect on the hh1 level. For the M-SL, the AlAsSb barrier centered in the InAsSb hole quantum well mainly pushes the hh1 level down. However, at shorter periods the effect of the barrier is also felt by the c1 state in the InAs electron quantum well, and thus also raises the c1 level. In the N-SL, the c1 level is affected in much the same way as in the M-SL. However, the hh1 level is actually raised slightly, since the AlAsSb layer acts to effectively widen the valence band quantum well (see Fig. 10).

Figure 12 shows the cutoff wavelength (calculated from band gap) as a function of superlattice period for several families of W-SL, M-SL, and N-SL

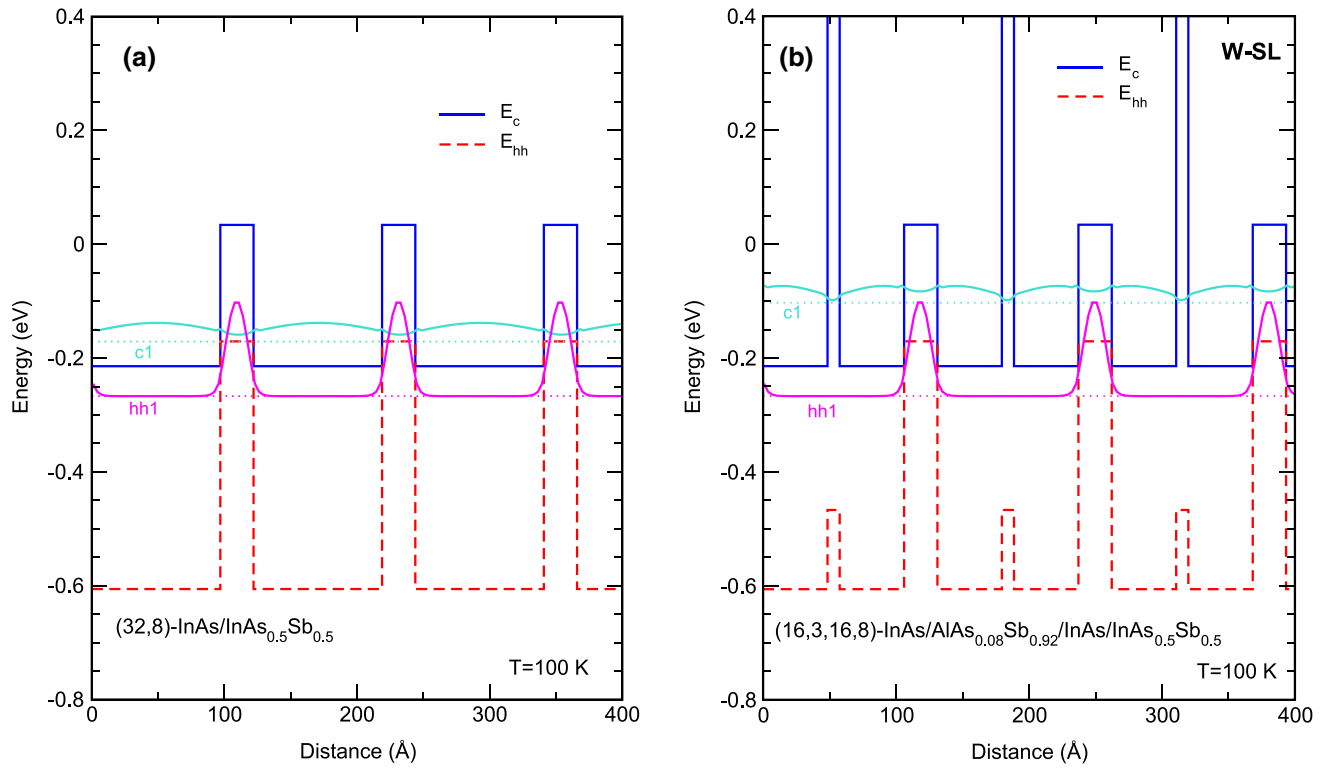


Fig. 9. Energy band diagrams, the $c1$ and $hh1$ band edge positions, and $c1$ and $hh1$ probability densities for: (a) the (32,8)-InAs/InAs_{0.5}Sb_{0.5} superlattice, and (b) a corresponding W-superlattice.

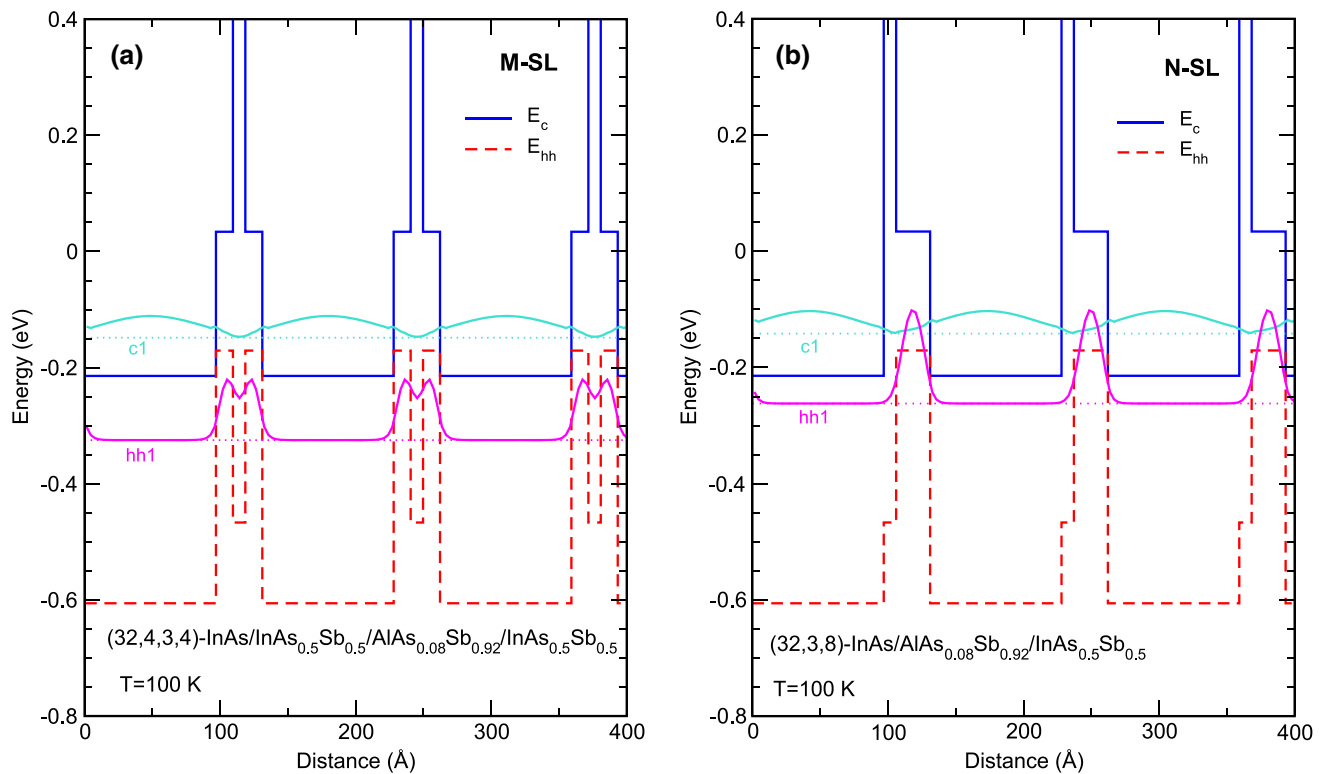


Fig. 10. Energy band diagrams, the $c1$ and $hh1$ band edge positions, and $c1$ and $hh1$ probability densities for: (a) an M-superlattice, and (b) an N-superlattice.

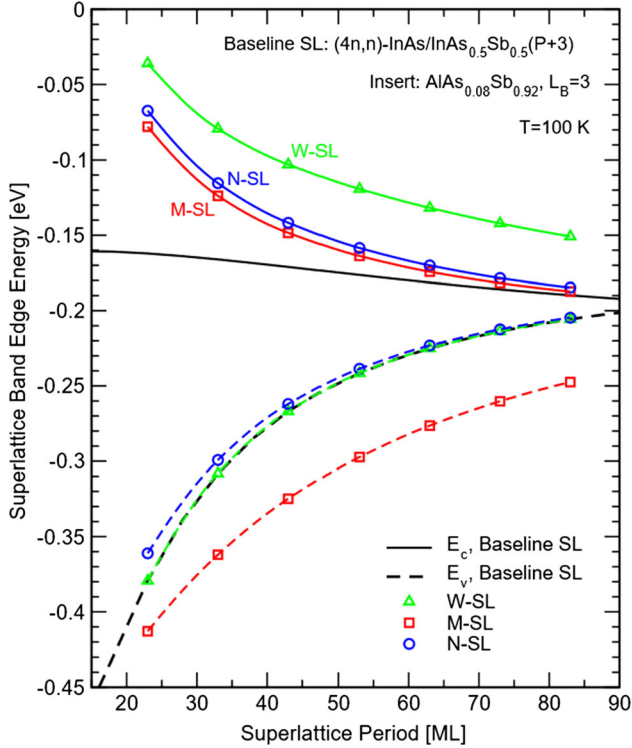


Fig. 11. Conduction and valence subband edges as functions of superlattice period for a family of (m,n) -InAs/InAs_{0.5}Sb_{0.5} superlattices, $m/n = 4$, and the corresponding W-, M-, and N-superlattices formed by the insertion of 3-monolayer thick AlAsSb barriers. For ease of comparison, the curves for the baseline (m,n) -InAs/InAs_{0.5}Sb_{0.5} superlattice have been shifted horizontally by 3 monolayers.

formed by inserting AlAsSb barriers of various thicknesses in the baseline (m,n) -InAs/InAs_{0.5}Sb_{0.5} superlattices. In all cases, the addition of even the thinnest AlAsSb barrier increases the period required to achieve the same cutoff wavelength; increasing the barrier thickness further increases the period. Figures 13 and 14 show the effect of the AlAsSb barrier on the growth-direction electron and hole conductivity effective masses direction $m_{n,z}^{**}$ and $m_{p,z}^{**}$ in W-SL, M-SL, and N-SL. In all cases, the presence of the barrier increases both $m_{n,z}^{**}$ and $m_{p,z}^{**}$. We compare specifically a baseline InAs/InAs_{0.5}Sb_{0.5} superlattice and the corresponding W-SL with 3-monolayer (ML) AlAsSb insertions, both with 12 μm cutoff wavelength. The baseline superlattice has a period $P = 38$ ML, $m_{n,z}^{**} = 0.029 m_0$, and $m_{p,z}^{**} = 6.5 m_0$, while the corresponding W-SL has $P = 59$ ML, $m_{n,z}^{**} = 0.036 m_0$, and $m_{p,z}^{**} = 142 m_0$. It is apparent that the advantage of increased electron-hole wavefunction overlap is eclipsed by the increase in superlattice period and growth-direction effective masses. Table I lists the numerical values of the superlattice band edges, band gaps, and the cutoff wavelengths for the specific cases depicted in Figs. 9 and 10.

The calculations described in this section use AlAsSb lattice-matched to GaSb substrate. A reviewer of this paper points out that if instead we

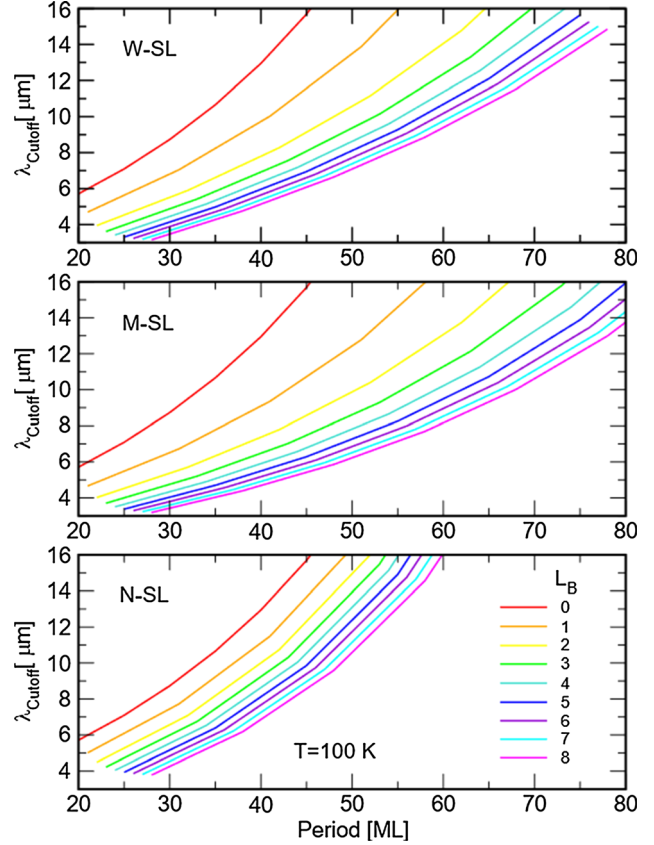


Fig. 12. Calculated cutoff wavelength as functions of superlattice period for several families of W-, M-, and N-superlattices formed by inserting AlAsSb barriers in the baseline (m,n) -InAs/InAs_{0.5}Sb_{0.5} superlattice. The barrier thickness L_B ranges from 0 to 8 monolayers.

used higher As fraction AlAsSb (which would be tensile on GaSb substrate), we could reduce the thickness of the tensile InAs layers in the superlattice and still achieve strain balance against the compressive InAsSb layers. This could potentially shorten the period required to achieve a given cutoff wavelength in the polytype superlattices. This is an interesting avenue for future investigation.

METAMORPHIC GROWTH

We mentioned that one challenge for the (V)LWIR InAs/InAsSb T2SLS is the relatively thick InAs layers required for strain balancing on GaSb substrate. This condition can be made more favorable if we can grow the InAs/InAsSb T2SLS on a virtual substrate with lattice constant larger than that of GaSb. The use of metamorphic buffer has enabled the extension of bulk InAsSb nBn detector cutoff wavelength from 4.2 μm to 5 μm ,²⁷ and could be beneficial for (V)LWIR InAs/InAsSb T2SLS detectors as well. We consider (m,n) -InAs/InAs_{0.5}Sb_{0.5} superlattices strain balanced on hypothetical GaInSb substrates of different compositions. Growing on GaSb substrate requires $m/n = 4$ for strain balancing. However, if we can grow on a Ga_{0.975}In_{0.025}Sb substrate, with a lattice constant

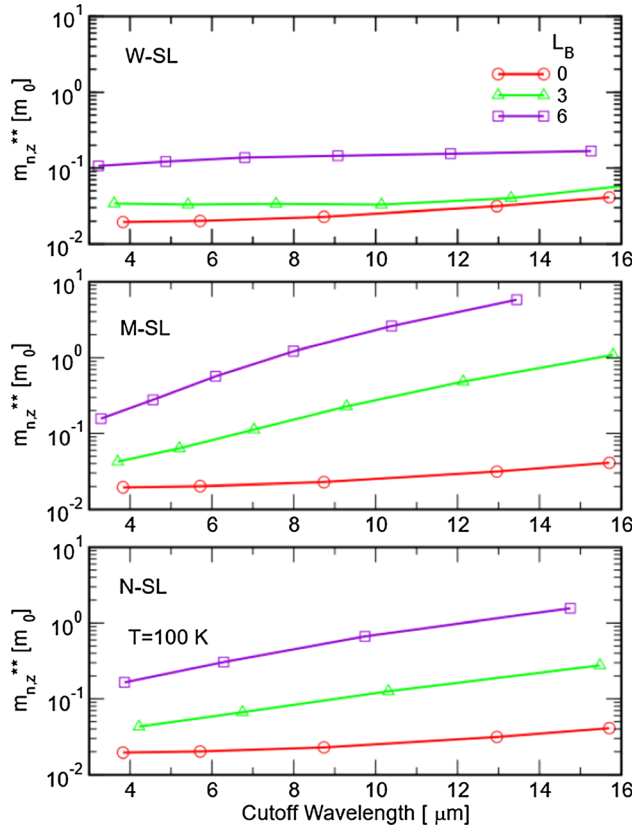


Fig. 13. Growth-direction electron conductivity effective masses as functions of cutoff wavelength for several families of W-, M-, and N-superlattices formed by inserting 3-ML and 6-ML thick AlAsSb barriers in the baseline (m,n) -InAs/InAs_{0.5}Sb_{0.5} superlattices.

0.16% larger than that of GaSb, then strain-balancing now requires $m/n = 3$. If we further increase the virtual substrate lattice constant to 0.43% larger than that of GaSb with $\text{Ga}_{0.932}\text{In}_{0.068}\text{Sb}$, we only require $m/n = 2$ for strain balancing. In practice, $\text{Ga}_{0.84}\text{In}_{0.14}\text{Sb}$ and $\text{Ga}_{0.7}\text{In}_{0.3}\text{Sb}$ virtual substrates,^{28,29} which have even higher In fraction, have already been demonstrated. Figure 15 shows that by growing on virtual substrates with even slightly larger lattice constants, we can reduce the superlattice period required to reach a given cutoff wavelength noticeably. Similarly, Fig. 16 shows that the growth-direction hole conductivity effective mass also decreases significantly. To be sure, the tradeoff for the advantages provided by the virtual substrates are in the need for metamorphic buffer growth, and in increased defect density.

SUMMARY

MWIR InAs/InAsSb superlattice has demonstrated excellent detector and FPA performance,^{3,4} with significantly higher operating temperature than the market-leading InSb. Compared to the InAs/GaSb superlattice, the InAs/InAsSb superlattice is easier to grow⁷ and has longer minority carrier lifetimes.⁸⁻¹⁰ However, for (V)LWIR, InAs/InAsSb requires longer superlattice period to

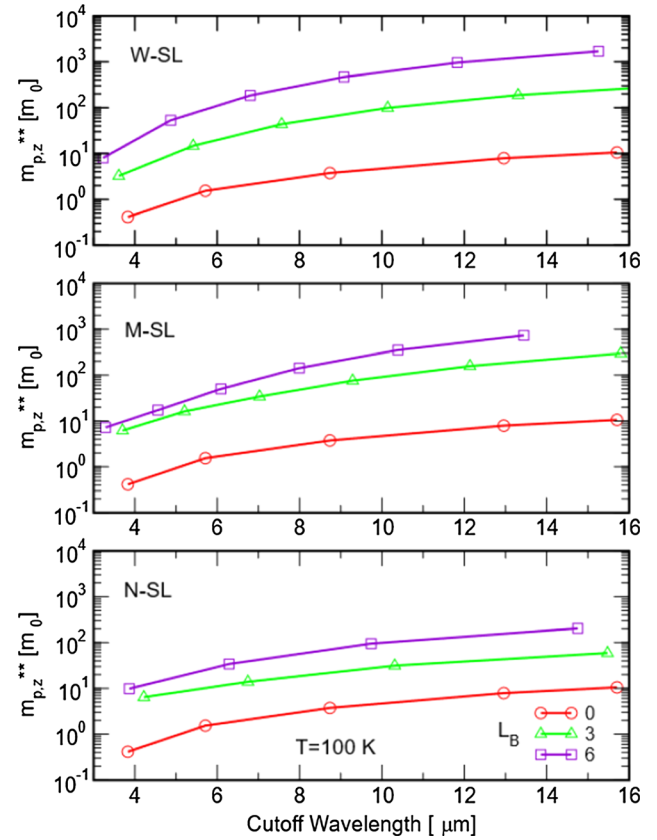


Fig. 14. Growth-direction hole conductivity effective masses as functions of cutoff wavelength for several families of W-, M-, and N-superlattices formed by inserting 3-ML and 6-ML thick AlAsSb barriers in the baseline (m,n) -InAs/InAs_{0.5}Sb_{0.5} superlattices.

achieve the same cutoff wavelength as InAs/GaSb, and therefore, has smaller absorption coefficients^{12,13} and larger growth-direction hole conductivity effective masses.^{14,15} While (V)LWIR InAs/InAsSb T2SLS FPAs have demonstrated high operability and uniformity, achieving good quantum efficiency has been more challenging. We explored some of the ideas to address these challenges for the InAs/InAsSb superlattice by theoretical modeling. We found that increasing the Sb fraction in the InAsSb alloy can reduce the InAs/InAsSb superlattice period significantly. At sufficiently high Sb fraction ($\sim 75\%$), InAs/InAsSb can match InAs/GaSb in terms of the superlattice period required to reach a given cutoff wavelength. However, high Sb fraction InAs/InAsSb superlattice are more prone to Sb segregation,¹⁹⁻²² which can negate the period-reduction benefit of high fraction Sb. Growth schemes that could reduce Sb segregation without introducing extra defects may be helpful in this matter. We also examined the cases where thin lattice-matched AlAsSb barrier layers are inserted in InAs/InAsSb to form polytype W, M, and N superlattices²³⁻²⁶ in order to increase electron-hole wavefunction overlap for stronger optical absorption. This strategy can be unfavorable because the presence of the AlAsSb barriers leads to increased

Table I. The c1 and hh1 band edge positions, band gaps, and cutoff wavelengths for the (32,8)-InAs/InAs_{0.5}Sb_{0.5} superlattice, and its corresponding W-SL, M-SL, and N-SL formed using 3-monolayer Al_{0.08}As_{0.92}Sb insertions

Superlattice	E_{c1} (eV)	E_{hh1} (eV)	E_g (eV)	λ_{cutoff} (μm)
(32,8)-InAs/InAs _{0.5} Sb _{0.5}	- 0.171	- 0.267	0.0958	12.9
W-SL	- 0.103	- 0.267	0.164	7.57
M-SL	- 0.148	- 0.325	0.176	7.03
N-SL	- 0.142	- 0.262	0.120	10.3

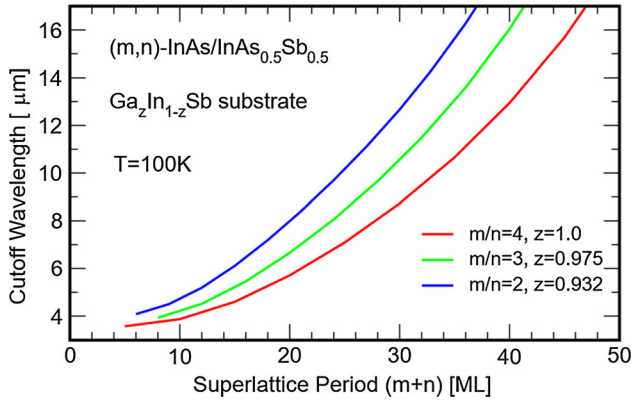


Fig. 15. Calculated cutoff wavelength as a function of superlattice period for families of (m,n) -InAs/InAs_{0.5}Sb_{0.5} superlattices strain balanced on hypothetical GaInSb substrates of different compositions.

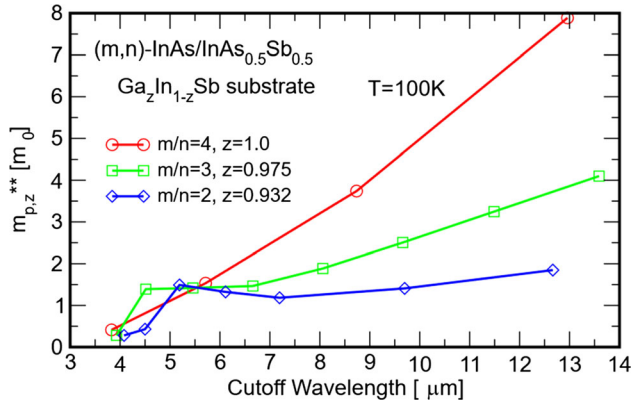


Fig. 16. Growth-direction hole conductivity effective masses as function of cutoff wavelength for families of (m,n) -InAs/InAs_{0.5}Sb_{0.5} superlattices strain balanced on hypothetical GaInSb substrates of different compositions.

band gap, and therefore, increases the superlattice period required to reach a given cutoff wavelength. Metamorphic growth on virtual substrates with larger lattice constants than GaSb can decrease the superlattice period needed to reach a specified cutoff wavelength, but this benefit should be weighed against the need for metamorphic buffer growth and the resulting higher defect density.

ACKNOWLEDGMENTS

The authors would like to thank S. Bandara, Y. Wei, R. Q. Yang, A. W. K. Liu, A. J. Ciani, and C. H.

Grein for helpful discussions. The research was carried out at the Jet Propulsion Laboratory, California Institute of Technology, under a contract with the National Aeronautics and Space Administration (80NM0018D004).

CONFLICT OF INTEREST

The authors declare that they have no conflict of interest.

REFERENCES

1. D.Z. Ting, A. Soibel, A. Khoshakhlagh, S.A. Keo, S.B. Rafol, A.M. Fisher, C.J. Hill, E.M. Luong, B.J. Pepper, and S.D. Gunapala, in *SPIE Proceedings, Infrared Technology and Applications XLV*, vol. 11002, p. 110020F (2019).
2. D.Z. Ting, A. Soibel, A. Khoshakhlagh, S.A. Keo, S.B. Rafol, L. Höglund, E.M. Luong, A.M. Fisher, C.J. Hill, and S.D. Gunapala, *J. Electron. Mater.* 48, 6145 (2019).
3. D.Z. Ting, A. Soibel, A. Khoshakhlagh, S.B. Rafol, S.A. Keo, L. Höglund, A.M. Fisher, E.M. Luong, and S.D. Gunapala, *Appl. Phys. Lett.* 113, 021101 (2018).
4. D.Z. Ting, S.B. Rafol, K.A. Sam, J. Nguyen, A. Khoshakhlagh, A. Soibel, L. Höglund, A.M. Fisher, E.M. Luong, J.M. Mumolo, J.K. Liu, and S.D. Gunapala, *IEEE Photonics J.* 10, 6804106 (2018).
5. M. Vuillermet, L. Rubaldo, F. Chabuel, C. Pautet, J.C. Terme, L. Mollard, J. Rothman, and N. Baier, in *SPIE Proceedings Infrared Technology and Applications XXXVII*, vol. 8012, p. 80122W (2011).
6. P. Klipstein, D. Aronov, M. Ezra, I. Barkai, E. Berkowicz, M. Brumer, R. Fraenkel, A. Glozman, S. Grossman, E. Jacobsohn, O. Klin, I. Lukomsky, L. Shkedy, I. Shtrichman, N. Snapi, M. Yassen, and E. Weiss, *Infrared Phys. Technol.* 59, 172 (2013).
7. D.Z. Ting, A. Khoshakhlagh, A. Soibel, C.J. Hill, and S.D. Gunapala, U. S. Patent No. 8,217,480 (2012).
8. E.H. Steenbergen, B.C. Connelly, G.D. Metcalfe, H. Shen, M. Wraback, D. Lubyshev, Y. Qiu, J.M. Fastenau, A.W.K. Liu, S. Elhamri, O.O. Cellek, and Y.-H. Zhang, *Appl. Phys. Lett.* 99, 251110 (2011).
9. B.V. Olson, E.A. Shaner, J.K. Kim, J.F. Klem, S.D. Hawkins, L.M. Murray, J.P. Prineas, M.E. Flatté, and T.F. Boggess, *Appl. Phys. Lett.* 101, 092109 (2012).
10. L. Höglund, D.Z. Ting, A. Khoshakhlagh, A. Soibel, C.J. Hill, A. Fisher, S. Keo, and S.D. Gunapala, *Appl. Phys. Lett.* 103, 221908 (2013).
11. D. Donetsky, S.P. Svensson, L.E. Vorobjev, and G. Belenky, *Appl. Phys. Lett.* 95, 212104 (2009).
12. P.C. Klipstein, Y. Livneh, A. Glozman, S. Grossman, O. Klin, N. Snapi, and E. Weiss, *J. Electron. Mater.* 43, 2984 (2014).
13. I. Vurgaftman, G. Belenky, Y. Lin, D. Donetsky, L. Shterengas, G. Kipshidze, W.L. Sarney, and S.P. Svensson, *Appl. Phys. Lett.* 108, 222101 (2016).
14. D.Z. Ting, A. Soibel, and S.D. Gunapala, *Appl. Phys. Lett.* 108, 183504 (2016).

15. D.Z. Ting, A. Soibel, and S.D. Gunapala, *Infrared Phys. Technol.* 84, 102 (2017).
16. Y.-C. Chang, *Phys. Rev. B* 37, 8215 (1988).
17. X. Cartoixa, D.Z.-Y. Ting, and T.C. McGill, *Phys. Rev. B* 68, 235319 (2003).
18. I. Vurgaftman, J.R. Meyer, and L.R. Ram-Mohan, *J. Appl. Phys.* 89, 5815 (2001).
19. A.J. Ciani, C.H. Grein, B. Irick, M.S. Miao, and N. Kioussis, *Opt. Eng.* 56, 091609 (2017).
20. H.J. Haugan, G.J. Brown, and J.A. Peoples, *J. Vac. Sci. Technol. B* 35, 02B107 (2017).
21. W.L. Sarney, S.P. Svensson, M.K. Yakes, Y. Xu, D. Donetsky, and G. Belenky, *J. Appl. Phys.* 124, 035304 (2018).
22. K. Kanedy, F. Lopez, M.R. Wood, C.F. Gmachl, M. Weimer, J.F. Klem, S.D. Hawkins, E.A. Shaner, and J.K. Kim, *Appl. Phys. Lett.* 112, 042105 (2018).
23. L. Esaki, L.L. Chang, and E.E. Mendez, *Jpn. J. Appl. Phys.* 20, L529 (1981).
24. C.L. Canedy, E.H. Aifer, I. Vurgaftman, J.G. Tischler, J.R. Meyer, J.H. Warner, and E.M. Jackson, *J. Electron. Mater.* 36, 852 (2007).
25. P.Y. Delaunay, B.M. Nguyen, D. Hoffman, E.K.W. Huang, and M. Razeghi, *IEEE J. Quantum Electron.* 45, 157 (2009).
26. O. Salihoglu, A. Muti, K. Kutluer, T. Tansel, R. Turan, Y. Ergun, and A. Aydinli, *Appl. Phys. Lett.* 101, 073505 (2012).
27. N. Baril, A. Brown, P. Maloney, M. Tidrow, D. Lubyshev, Y. Qiu, J.M. Fastenau, A.W.K. Liu, and S. Bandara, *Appl. Phys. Lett.* 109, 122104 (2016).
28. G. Kipshidze, T. Hosoda, W.L. Sarney, L. Shterengas, and G. Belenky, *IEEE Photon Technol. Lett.* 23, 317 (2011).
29. D. Wang, Y. Lin, D. Donetsky, L. Shterengas, G. Kipshidze, G. Belenky, W.L. Sarney, H. Hier, and S.P. Svensson, in *SPIE Proceedings Infrared Technology and Applications XXXVIII*, vol. 8353, p. 835312 (2012).

Publisher's Note Springer Nature remains neutral with regard to jurisdictional claims in published maps and institutional affiliations.